Medical Physics
The International Journal of Medical Physics Research and Practice

Development of a physical 3D anthropomorphic breast phantom

Ann-Katherine Carton, Predrag Bakic, Christer Ullberg, Helen Derand, and Andrew D. A. Maidment

Citation: Medical Physics **38**, 891 (2011); doi: 10.1118/1.3533896
View online: http://dx.doi.org/10.1118/1.3533896
View Table of Contents: http://scitation.aip.org/content/aapm/journal/medphys/38/2?ver=pdfcov
Published by the American Association of Physicists in Medicine

Development of a physical 3D anthropomorphic breast phantom

Ann-Katherine Carton[a] and Predrag Bakic
Department of Radiology, University of Pennsylvania, 1 Silverstein Building, 3400 Spruce Street, Philadelphia, Pennsylvania 19104-4206

Christer Ullberg[b] and Helen Derand[b]
XCounter AB, Svärdvägen 11, SE-182 33 Danderyd, Sweden

Andrew D. A. Maidment
Department of Radiology, University of Pennsylvania, 1 Silverstein Building, 3400 Spruce Street, Philadelphia, Pennsylvania 19104-4206

(Received 11 June 2010; revised 5 October 2010; accepted for publication 24 November 2010; published 24 January 2011)

Purpose: Develop a technique to fabricate a 3D anthropomorphic breast phantom with known ground truth for image quality assessment of 2D and 3D breast x-ray imaging systems.
Methods: The phantom design is based on an existing computer model that can generate breast voxel phantoms of varying composition, size, and shape. The physical phantom is produced in two steps. First, the portion of the voxel phantom consisting of the glandular tissue, skin, and Cooper's ligaments is separated into sections. These sections are then fabricated by high-resolution rapid prototyping using a single material with 50% glandular equivalence. The remaining adipose compartments are then filled using an epoxy-based resin (EBR) with 100% adipose equivalence. The phantom sections are stacked to form the physical anthropomorphic phantom.
Results: The authors fabricated a prototype phantom corresponding to a 450 ml breast with 45% dense tissue, deformed to a 5 cm compressed thickness. Both the rapid prototype (RP) and EBR phantom materials are radiographically uniform. The coefficient of variation (CoV) of the relative attenuation between RP and EBR phantom samples was $<1\%$ and the CoV of the signal intensity within RP and EBR phantom samples was $<1.5\%$ on average. Digital mammography and reconstructed digital breast tomosynthesis images of the authors' phantom were reviewed by two radiologists; they reported that the images are similar in appearance to clinical images, noting there are still artifacts from air bubbles in the EBR.
Conclusions: The authors have developed a technique to produce 3D anthropomorphic breast phantoms with known ground truth, yielding highly realistic x-ray images. Such phantoms may serve both qualitative and quantitative performance assessments for 2D and 3D breast x-ray imaging systems. [DOI: 10.1118/1.3533896]

Key words: breast x-ray imaging, anthropomorphic breast phantom, image quality assessment, digital breast tomosynthesis, mammography

I. INTRODUCTION

Physical phantoms are essential tools to assess and optimize image quality in breast x-ray imaging systems. Typical phantoms consist of a homogenous material in which appropriate test objects are embedded. Such geometric phantoms are used to evaluate high-contrast and low-contrast object detectability, subject contrast, phototimer performance, linearity of the detector response, spatial resolution, and noise response. However, more realistic imaging tasks require an anthropomorphic breast phantom, i.e., a tissue equivalent phantom providing x-ray images similar to those of a real breast.

The only commercially available anthropomorphic breast phantom is the "Rachel" phantom (Gammex 169, Gammex Inc., Middleton, WI),[1] which has gained wide acceptance for the evaluation of 2D mammography systems. This phantom consists of a breast tissue equivalent base aligned over a mercury intensified film image. The base simulates the coarse tissue structures, while the film image simulates fine tissue details. A radiographic projection through the phantom resembles a mammogram, provided the acquisition geometry is consistent with the geometry for which the phantom was designed.[1] The application of the Rachel phantom is limited to the evaluation of 2D projection imaging systems[1,2] because this phantom does not simulate the 3D anatomy of the breast.

With the introduction of novel 3D breast x-ray imaging systems, including digital breast tomosynthesis (DBT) and breast computed tomography, there is an increasing need for a high-resolution, 3D anthropomorphic breast phantom with known ground truth. Such a phantom would permit a controlled evaluation of various tomographic reconstruction techniques for a wide range of image quality parameters including noise, contrast, reconstruction artifacts, and geometric distortions, as well as the optimization of image acquisition parameters (e.g., the number and spacing of projection images and angular range). A 3D anthropomorphic breast phantom could also be used to evaluate and compare the performance across 2D and 3D x-ray imaging modalities.

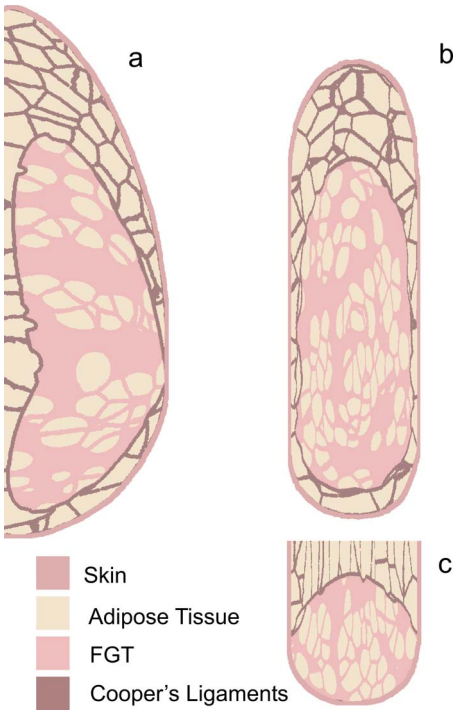

FIG. 1. Orthogonal slices through the breast voxel phantom used as 307 the design of our prototype physical phantom. The sections were made after simulating the breast compression. (a) Axial, (b) coronal, and (c) sagittal phantom slices were made after simulating the breast compression.

The purpose of our study was to develop a technique to fabricate a 3D physical anthropomorphic breast phantom. The phantom design, material selection, and fabrication process are described. Digital mammography (DM) and reconstructed DBT images of the phantom are presented.

II. MATERIALS AND METHODS

II.A. General phantom design

The phantom design is based on an existing computer model that can generate breast voxel phantoms of varying composition, size, and shape[3–6] (Fig. 1). Briefly, the voxel phantom consists of two large scale regions. The inner region is composed of fibroglandular tissue, in which medium scale compartments of adipose tissue are embedded. The outer region is composed of adipose tissue organized into medium scale compartments supported by a matrix representing the Cooper's ligaments. The phantom is covered by a layer of skin. The deformation of the breast during mammography or digital breast tomosynthesis is simulated using a finite element tissue model.[7]

Prior to phantom fabrication, the four tissue types in the voxel phantom are divided into two classes determined by the fabrication technique and phantom materials. The first class consists of fibroglandular tissue, skin, and Cooper's ligaments; these tissues are fabricated by rapid prototyping using a single tissue equivalent material. The second class consists of adipose tissue which is fabricated using an epoxy-based resin (EBR) that is manually cast in the compartments of the rapid prototype (RP) product.

The following preprocessing steps are performed. First, morphological dilation with a spherical structural element of radius equal to 3 voxels is applied to the voxel phantom composed of fibroglandular tissue, skin, and Cooper's ligaments to ensure that the Cooper's ligaments are continuous and provide structural stability. Next, the voxel phantom is separated into sections to expose the adipose tissue compartments in the RP product so they can later be filled with EBR. The voxel phantom composed of fibroglandular tissue, skin, and Cooper's ligaments is then converted to a stereolithography (STL) data format required for rapid prototyping. We performed the tissue labeling, section slicing, surface modeling, and STL conversion using MIMICS software (Materialise NV, Leuven, Belgium).

II.B. Phantom materials

FC-720 (Objet Geometries Ltd., Rehovot, Israel), an acrylic-based photopolymer, is used to create the fibroglandular tissue, skin, and Cooper's ligaments. FC-720 was selected because of its durability, strength, and radiographic properties. FC-720 was the most radiographically dense of the four commercially available RP materials we compiled; it is equivalent to 50% glandular tissue. The three other investigated materials are FC-830, FC-840, and FC-850 (Objet Geometries Ltd., Rehovot, Israel).

An EBR with 100% adipose equivalency was developed to create the adipose tissue. The EBR is composed of 74% Araldite CY221 resin (Huntsman, Everberg, Belgium), 13% HY956 Eu hardener (Huntsman, Everberg, Belgium), and 12% phenolic microspheres (Chance and Hunt Limited, Cheshire, U.K.), by mass. We fabricated the EBR using a method similar to that described previously.[8]

The glandular equivalency and radiographic uniformity of the phantom materials were experimentally assessed from signal intensity (SI) measurements in images acquired with a Selenia Dimensions DBT machine (Hologic Inc., Bedford, MA). These characteristics were assessed using 1 cm thick RP and EBR phantom samples and 1 cm thick tissue equivalent samples with known glandularity (CIRS, Norfolk, VA). The samples were imaged using a W/Rh target/filter x-ray beam at tube voltages from 22 to 32 kV. SI measurements were performed in linear projection images after flat-field and offset corrections were applied by the manufacturer.

The glandular equivalency of the phantom materials was measured in terms of the primary attenuation of the phantom materials relative to tissue equivalent materials with known glandularity. The relative attenuation R was computed as

$$R(E) = \frac{\overline{\mathrm{SI}}_p(E) - \overline{\mathrm{SI}}_g(E)}{\overline{\mathrm{SI}}_g(E)} \times 100\%,$$

where $\overline{\mathrm{SI}}_p(E)$ and $\overline{\mathrm{SI}}_g(E)$ are the means in the per-pixel signal intensity at tube voltage E in images of the RP or EBR phantom sample p and in images of the breast tissue equivalent material g with known glandularity. The tissue equivalent materials had glandularities ranging from 0% to 100% (CIRS, Norfolk, VA). Samples of phantom material and of tissue equivalent material with known glandularity were im-

aged simultaneously to eliminate confounding variations in SI due to temporal changes in tube output and detector sensitivity. In preliminary experiments, we found that detector sensitivity varies slightly as a function of position. Therefore, a set of extra exposures was made without samples in the beam to provide a reference signal from which the actual measurements were corrected. The mean SI difference between two test regions served to correct the measurements for spatial sensitivity variations. A narrow beam geometry was used to limit the influence of scattered radiation. A 1.8 mm thick Pb plate, resulting in a primary transmission less than 10^{-4}% for a 28 kV W/Rh target/filter x-ray beam, was placed approximately 1.5 cm below the exit port of the x-ray tube. The Pb plate contained two circular apertures that defined the test regions. The projected test regions were 3 cm in diameter at the detector; they were located symmetrically about the midline of the detector 7 cm apart and 5 cm from the chest wall. The mean SI was computed in 1 cm diameter circular regions centered in the test regions.

The radiographic uniformity was assessed both between and within phantom samples. To characterize the radiographic uniformity between phantom samples, the attenuation of ten RP or ten EBR phantom samples p was measured relative to the attenuation of a reference material r. The reference material was simultaneously imaged with each of the phantom samples using an experimental setup similar to that described for the assessment of the glandular equivalency. The relative attenuation was measured as $\overline{\mathrm{SI}}_p(E)/\overline{\mathrm{SI}}_r(E) \times \langle \overline{\mathrm{SI}}_r(E) \rangle$, where $\langle \overline{\mathrm{SI}}_r(E) \rangle$ represents the average attenuation of the reference material over ten exposures and accounts for the variations in x-ray intensities between exposures. The coefficient of variation (CoV) (the ratio of the standard deviation to the mean) of the relative attenuation was computed as a measure for the radiographic uniformity between phantom samples. The CoV of the per-pixel SI for each phantom sample was computed as a measure for the radiographic uniformity within each phantom sample. The radiographic uniformity of the RP and EBR phantom materials was compared to the radiographic uniformity of commercial 100% adipose tissue equivalent samples. The mean and standard deviation in SI were computed in 1 cm diameter circular regions centered in the FOV of the x-ray fields.

II.C. Phantom fabrication

The sections of fibroglandular tissue, Cooper's ligaments, and skin were fabricated using rapid prototyping, a technology that creates 3D objects by fabricating successive layers of material. We used a polyjet Eden 500V printer (Objet, Rehovot, Israel) to deposit liquid FC-720 photopolymer, layer by layer, according to the model of the fibroglandular tissue region, the matrix of Cooper's ligaments, and skin layer. An auxiliary material is deposited in the adipose tissue compartments to support overhanging layers of the model. This support material is removed by a high pressure water stream after the photopolymer is cured. The sections are printed using a voxel resolution of 60 μm. Residual support material was manually removed with a scalpel and a hard acid brush.

Next, a thin primer, consisting of a mixture of Araldite CY221 resin and HY 956 Eu hardener (5 to 1 mass ratio), was applied to the surface of the adipose tissue compartments. Then, the adipose tissue compartments were filled with EBR. The EBR was poured in ~1 mm thick layers to allow air bubbles to escape from the highly viscous EBR. Each layer was left to cure before the next was applied. Periodically throughout this process, radiographs of the phantom sections were acquired to localize remaining air bubbles; the largest bubbles (~0.5 mm in diameter) were broken with a needle before the next layer was poured.

Finally, the phantom sections were sanded using P180 grit sandpaper to remove excess EBR. The phantom sections were then stacked together.

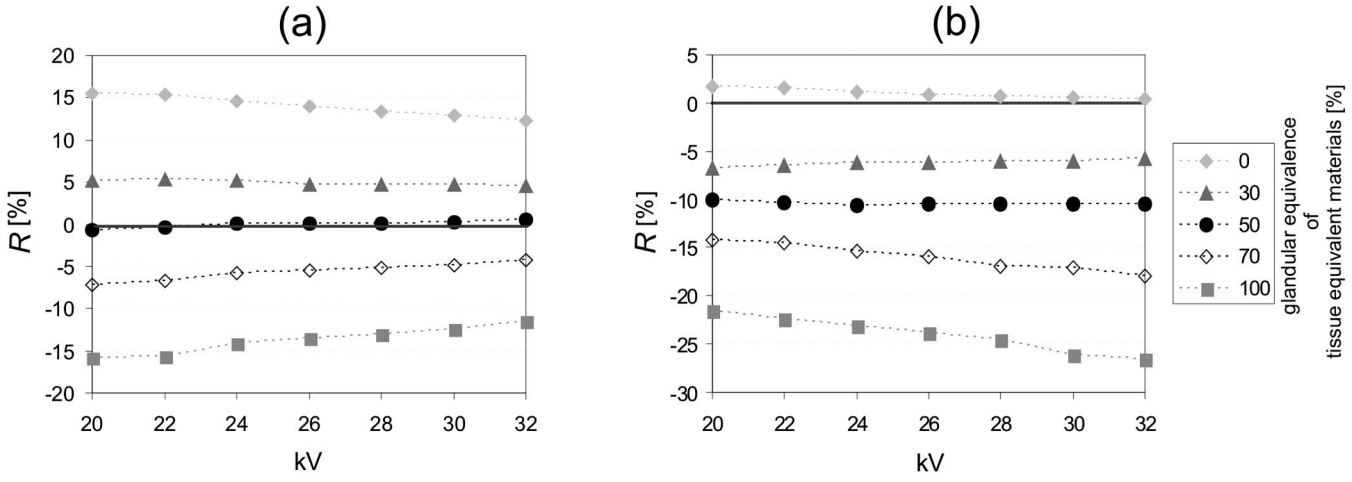

FIG. 2. R of (a) RP and (b) EBR phantom materials as a function of kV. When $R=0$ (indicated by the black line), the phantom materials have the same glandular equivalence as the tissue equivalent materials with known glandular equivalence.

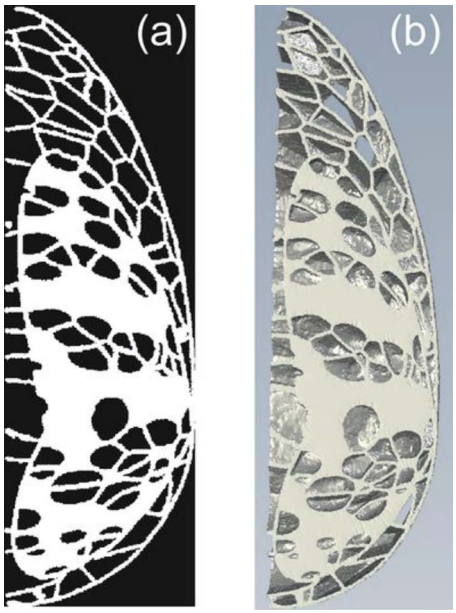

FIG. 3. (a) Tomographic slice of the voxel phantom composed of fibroglandular tissue, skin, and Cooper's ligament, corresponding to the slice of the voxel phantom shown in Fig. 1. (b) A 1 cm thick section of the voxel phantom ready for rapid prototyping.

III. RESULTS

III.A. Phantom materials

Figures 2(a) and 2(b) show the glandular equivalency (i.e., relative attenuation) as a function of kV for the RP and EBR phantom materials, respectively. These figures show that the RP and the EBR phantom materials are 50% and 0% glandular equivalent (100% adipose equivalent), respectively.

The CoV of the relative attenuation of the various phantom samples was 0.3% and 0.8% for the ten RP and the ten EBR samples, respectively. By comparison, the CoV of the relative attenuation of the commercial 100% adipose tissue equivalent material was 0.1%.

The CoV of the per-pixel SI was 1.10% on average (range: 1.07%–1.14%) for the ten RP samples and 1.30% on average (range: 0.9%–1.37%) for the ten EBR phantom samples. By comparison, the CoV of the per-pixel SI was 1.09% on average (range: 1.07%–1.11%) for the ten 100% adipose tissue equivalent samples.

III.B. Prototype phantom

We have fabricated one prototype anthropomorphic breast phantom for image quality assessment in DBT and mammography. The voxel phantom used to construct this prototype phantom has a volume of 450 ml and corresponds to a B cup breast size (Fig. 1). The phantom was deformed to a 5 cm compressed thickness. The voxel phantom was created with 200 μm^3 spatial resolution. Radiographically dense tissue is defined as the fraction of the fibroglandular tissue and Cooper's ligaments to the total breast tissue. After dilation of the Cooper's ligaments, the voxel phantom is composed of 45% and 47% radiographically dense tissue, by volume and by mass, respectively.

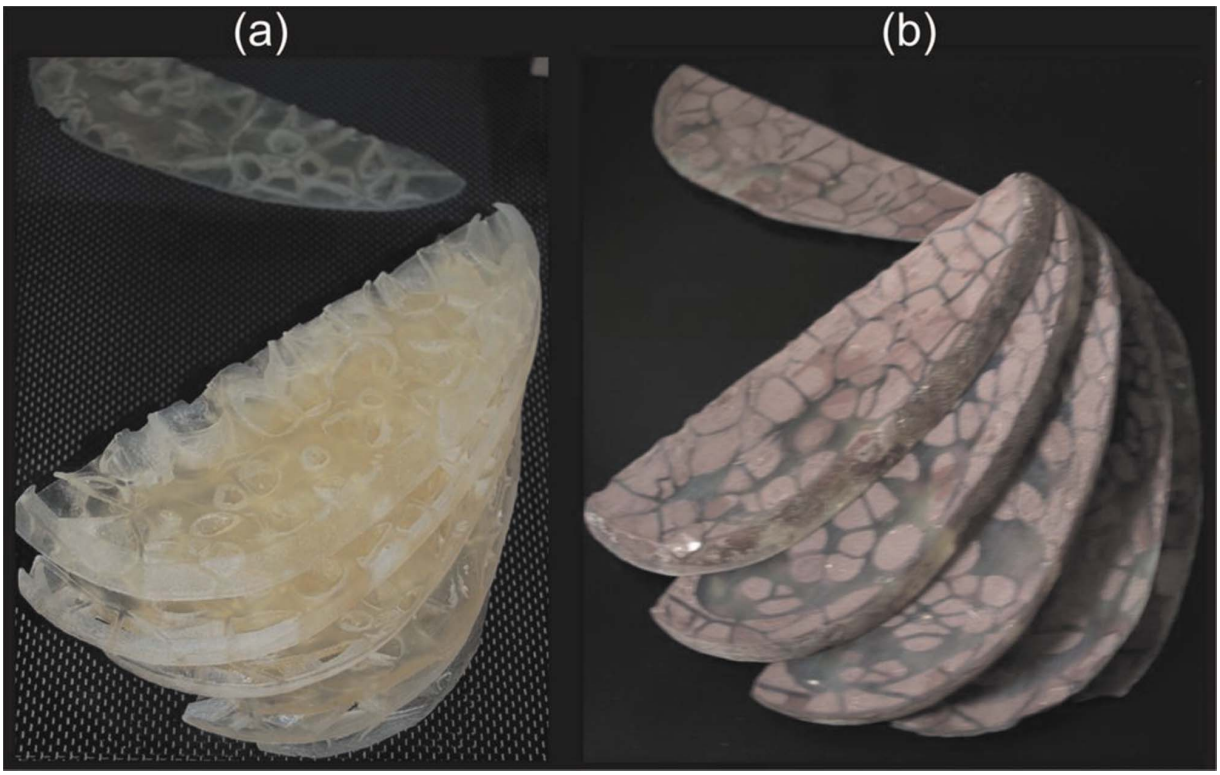

FIG. 4. (a) Phantom sections of the fibroglandular tissue, skin, and Cooper's ligaments fabricated using RP in single tissue equivalent materials. (b) Phantom sections after filling the RP printouts with the EBR.

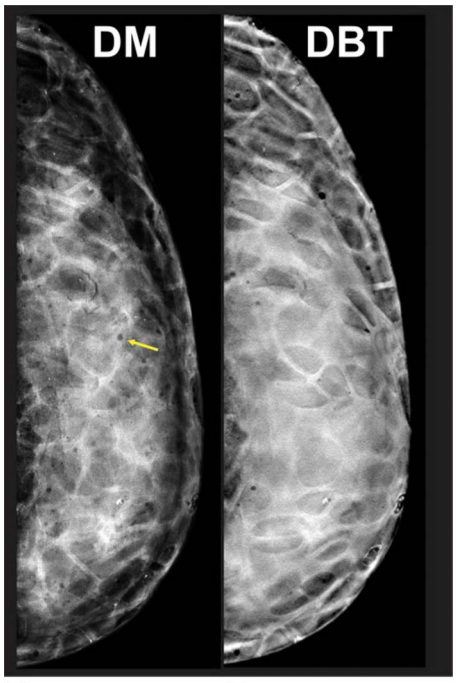

FIG. 5. (a) DM and (b) reconstructed DBT images of our prototype 3D physical anthropomorphic breast phantom. DM and DBT projection images were acquired with the autofilter AEC technique used for patient imaging. Note the occurrence of air bubbles in the epoxy, seen as radiolucent spheres (arrow).

The voxel phantom was constructed in six sections; the two outer sections are 0.5 cm thick and the remaining four inner sections are 1 cm thick. These section thicknesses, the adipose tissue compartments of the RP product were exposed so that they could be filled with the EBR. Figure 3(a) shows a tomographic slice of the voxel phantom composed of fibroglandular tissue, Cooper's ligaments, and skin. Figure 3(b) shows a 1 cm thick section of the voxel phantom composed of fibroglandular tissue, Cooper's ligaments, and skin, given as input to the RP printer.

Figure 4(a) shows the six FC-720 RP sections representing the fibroglandular tissue, Cooper's ligaments, and skin. Figure 4(b) shows the completed phantom with the RP sections filled with EBR. The phantom fabrication was completed by aligning and stacking the six sections.

To evaluate the prototype phantom, it was imaged with the same DBT system used for the characterization of the phantom materials. Figure 5(a) shows a DM image of our phantom. This image was acquired using the "autofilter" automatic exposure control (AEC) setting (W/Rh target/filter, 30 kV, 104 mA s). Figure 5(b) shows a reconstructed DBT image of the phantom. The DBT projection images were acquired using the autofilter AEC setting (W/Rh target/filter, 32 kV, 52 mA s). The DBT projection series consisted of 15 images acquired in 1° increments over a 15° arc. The DBT projection image series was reconstructed using a filtered-backprojection algorithm provided by the manufacturer. The images were reconstructed in planes parallel to the detector, in 1 mm increments, with an in-plane voxel pitch of 140 μm. The DM and DBT images were written as DICOM objects to a Hologic research workstation (SecurView DX, Hologic, Bedford, MA) used for both DM and DBT. The images were assessed by two MQSA certified radiologists. The DBT images were viewed in stack mode. The two radiologists reported that the DM and DBT images simulate a dense fibroglandular pattern that appears qualitatively similar to that of clinical images and that the grayscale range of adipose and fibroglandular elements approximates the pattern seen in a heterogeneously dense breast, noting there are still artifacts from air bubbles in the EBR as indicated by the arrows on Figs. 5(a) and 5(b).

IV. DISCUSSION

To assess the performance of novel 3D breast x-ray imaging systems, there is an increasing need for a physical phantom simulating 3D anatomy of the breast with high anatomical detail. DBT and mammography images of the prototype 3D anthropomorphic phantom described here have a qualitatively similar appearance to clinical images. With known ground truth in the form of a companion voxel phantom, we believe this phantom makes an excellent tool for both qualitative and quantitative assessment of the image quality across various DBT and mammography systems.

The spatial resolution of the voxel phantom (200 μm^3 voxels) used as the design for our prototype physical phantom is approximately 3.3 times larger than the RP print resolution (60 μm^3); the latter corresponds to the limiting spatial resolution of breast x-ray imaging detectors. Due to memory limitations of our current software, we were not able to simulate higher resolution voxel phantoms. Work is underway to optimize the software architecture so that we can simulate higher resolution phantoms.

The prototype phantom is not an exact replica of the companion voxel phantom. First, the EBR has some residual air bubbles that are visible on the radiographs. The air bubbles can be attributed to the high viscosity of the EBR and the fact that the resin could not be cast while under vacuum. Second, manual cleaning of the support material and sanding of the phantom sections may have resulted in slight differences from the numerical voxel phantom.

The current fabrication method is time-consuming. A more accurate and efficient manufacturing technique is clearly required. In case the fabrication technique described above would be used to fabricate future phantoms, additional steps will have to be taken to remove bubbles. The most obvious option would be to fabricate the complete phantom in a single process using RP technology. This would require that multiple materials of different composition simulating the various tissue types become readily available.

Today, phantoms with a radiographic density equivalent to 50% glandular tissue are employed in quality assurance programs and for optimization and dosimetry of mammography systems. However, in the future, physical phantoms with a lower radiographic density might be preferable because they better resemble the average breast density of women in the screening population. For instance, Young *et al.*[9] have

shown that the average volume percentage of dense tissue corresponds to 35% for a 5 cm thick compressed breast for women between 49 to 60 yr. Similar densities were reported by Geise *et al.*[10] In a recent publication of Yaffe *et al.*,[11] the average breast density of a screening population was found to be as low as 19.3%. The density of our edited voxel phantom is 45% in volume. However, since the radiographic density of our RP material is equivalent to 50% glandular tissue, the radiographic equivalence of our physical phantom is smaller than the 45% glandular tissue equivalent. Thus, our phantom resembles more realistically the average breast density. We continue to search for a more attenuating material so that the radiographic density of future phantoms would match the actual density of the corresponding voxel phantom.

The next phantom should include an interlocking system to ensure proper alignment of the stacked sections. The phantom could also be provided with one or more extra sections, modified to include simulated microcalcifications, fibers, masses, or hollow tumors accessible externally through tubes.[12]

In summary, we have developed a technique to fabricate a 3D anthropomorphic breast phantom. The phantom could be of use to test the performance of 2D and 3D breast x-ray imaging systems. A unique feature of the physical phantom is that it has a computational "twin." This combined system of physical and computational phantoms allows for both qualitative and quantitative image quality assessment.

ACKNOWLEDGMENTS

The authors acknowledge the financial support of Xcounter AB (Danderyd, Sweden) and Hologic Inc. (Bedford, MA). The authors would like to thank Dr. Emily Conant and Dr. Sara Gavenonis for reviewing the phantom images.

[a]Author to whom correspondence should be addressed. Electronic mail: andrew.maidment@uphs.upenn.edu; Telephone: 215 746 8763; Fax: 215 746 8764.
[b]Telephone: +46 8 622 2300; Fax: +46 8 622 23 12.

[1]C. B. Caldwell and M. J. Yaffe, "Development of an anthropomorphic breast phantom," Med. Phys. **17**, 273–280 (1990).
[2]C. B. Caldwell, E. K. Fishell, R. A. Jong, W. J. Weiser, and M. J. Yaffe, "Evaluation of mammographic image quality: Pilot study comparing five methods," AJR, Am. J. Roentgenol. **159**, 295–301 (1992).
[3]C. Zhang, P. R. Bakic, and A. D. A. Maidment, "Development of an anthropomorphic breast software phantom based on region growing algorithm," in *Proceedings of the Medical Imaging Conference 2008: Visualization, Image-guided Procedures, and Modeling (volume 6918)*, 69180V, edited by M. I. Miga and K. R. Cleary (SPIE, San Diego, CA, 2008).
[4]P. R. Bakic, M. Albert, D. Brzakovic, and A. D. A. Maidment, "Mammogram synthesis using a 3D simulation. II. Evaluation of synthetic mammogram texture," Med. Phys. **29**, 2140–2151 (2002).
[5]P. R. Bakic, M. Albert, D. Brzakovic, and A. D. A. Maidment, "Mammogram synthesis using a 3D simulation. I. Breast tissue model and image acquisition simulation," Med. Phys. **29**, 2131–2139 (2002).
[6]P. R. Bakic, M. Albert, D. Brzakovic, and A. D. A. Maidment, "Mammogram synthesis using a three-dimensional simulation. III. Modeling and evaluation of the breast ductal network," Med. Phys. **30**, 1914–1925 (2003).
[7]N. V. Ruiter, C. Zhang, P. R. Bakic, A.-K. Carton, J. Kuo, and A. D. A. Maidment, "Simulation of tomosynthesis images based on an anthropomorphic software breast tissue phantom," in *Proceedings of the Medical Imaging Conference 2008: Visualization, Image-guided Procedures, and Modeling (volume 6918)*, 69182I, edited by M. I. Miga and K. R. Cleary(SPIE, San Diego, CA, 2008).
[8]D. R. White, R. J. Martin, and R. Darlison, "Epoxy resin based tissue substitutes," Br. J. Radiol. **50**, 814–821 (1977).
[9]K. C. Young, M. L. Ramsdale, and F. Bignell, "Review of dosimetric methods for mammography in the UK breast screening programme," Radiat. Prot. Dosim. **80**, 183–186 (1998).
[10]R. A. Geise and A. Palchevsky, "Composition of mammographic phantom materials," Radiology **198**, 347–350 (1996).
[11]M. J. Yaffe, J. M. Boone, N. Packard, O. Alonzo-Proulx, S.-Y. Huang, C. L. Peressotti, A. Al-Mayah, and K. Brock, "The myth of the 50–50 breast," Med. Phys. **36**, 5437–5443 (2009).
[12]A.-K. Carton, B. Bakic, C. Ullberg, and A. D. A. Maidment, "Development of a 3D high-resolution physical anthropomorphic breast phantom," in *Proceedings of the Medical Imaging Conference 2010: Physical of Medical Imaging (volume 7622)*, edited by E. Samei and N. J. Pelc (SPIE, San Diego, CA, 2008).